Ab initio simulations of geometrical frustration in supercooled liquid Fe and Fe-based metallic glass

P. Ganesh and M. Widom
Department of Physics, Carnegie Mellon University, Pittsburgh, Pennsylvania 15213, USA
(Received 18 January 2007; published 16 January 2008)

We investigate short range order in liquid and supercooled liquid Fe and Fe-based metallic glass using *ab initio* simulation methods. We analyze the data to quantify the degree of local icosahedral and polytetrahedral order and to understand the role of alloying in controlling the degree of geometric frustration. Comparing elemental Fe to Cu [P. Ganesh and M. Widom, Phys. Rev. B **74**, 134205 (2006)] we find that the degree of icosahedral order is greater in Fe than in Cu, possibly because icosahedral disclination line defects are more easily incorporated into bcc environments than fcc. In Fe-based metallic glass-forming alloys (FeB and FeZrB) we find that introducing small concentrations of small B atoms and large Zr atoms controls the frustration of local icosahedral order.

DOI: 10.1103/PhysRevB.77.014205 PACS number(s): 61.43.Dq, 61.25.Mv, 61.20.Ja, 31.15.A−

I. INTRODUCTION

As noted by Frank,[1] the local icosahedral clustering of 12 atoms about a sphere is energetically preferred because it is made up entirely of four-atom tetrahedra, the densest-packed cluster possible. However, local icosahedral order cannot be propagated throughout space without introducing defects. Frustration of packing icosahedra is relieved in a curved space, where a perfect 12-coordinated icosahedral packing exists.[2–4] We adopt this structure as an ideal reference against which actual configurations will be compared.

Disclination line defects of type ±72° may be introduced into this icosahedral crystal and thereby control the curvature. In order to "flatten" the structure and embed it in ordinary three dimensional space an excess of −72° disclinations is needed, and these cause increased coordination numbers of 14, 15 or 16. Large atoms, if present, would naturally assume high coordination numbers and aid in the formation of a disclination line network. Similarly, smaller atoms would naturally assume low coordination numbers of 8, 9, or 10, and have positive disclinations attached to them, increasing the frustration. For a particular coordination number, it may be possible to construct a cluster, known as a Kasper polyhedron (see Sec. III C), made entirely of tetrahedrons.

Honeycutt and Andersen[5] introduced a method to count the number of tetrahedra surrounding an interatomic bond. This number is 5 for icosahedral order with no disclination, 6 for a −72° disclination and 4 for a +72° disclination. Steinhardt, Nelson and Ronchetti[6] introduced the orientational order parameter $\hat{W}_6$ to demonstrate short range icosahedral order. We employ both methods to analyze icosahedral order in supercooled metals and metal alloys, in addition to conventional radial distribution functions, structure factors and Voronoi analysis.

Many simulations have been performed on pure elemental metals and metal alloys using model potentials,[7–10] but do not necessarily produce reliable structures owing to their imperfect description of interatomic interactions. First principles (*ab initio*) calculations achieve the most realistic possible structures, unhindered by the intrinsic inaccuracy of phenomenological potentials and with the ability to accurately capture the chemical natures of different elements and alloys. The tradeoff for increased accuracy is a decrease in the system sizes one can study, so only local order can be observed, not long range. Also runs are limited to short time scales. Early *ab initio* studies on liquid copper[11–13] and iron[14] were not analyzed from the perspective of icosahedral ordering. Recent *ab initio* studies on Ni and Zr[15,16] find that the degree of icosahedral ordering increases with supercooling in Ni, while in Zr bcc is more favored. Studies on binary metal alloys by Jakse *et al.*[17,18] and by Sheng *et al.*[19] quantify local icosahedral order in the alloys. We previously[20] investigated icosahedral order in liquid and supercooled Cu.

Elemental metals crystallize so easily that they can hardly be made amorphous at any quench rate. Alloying can improve the ease of glass formation. For some special alloys, a bulk amorphous state can be reached by slow cooling. Pure elemental Fe is a poor glass former, but Fe-based compounds like FeB and especially FeZrB, show improved glass formability. We augment our molecular-dynamics simulation with another algorithm called "tempering" or "replica exchange method" (REM)[21,22] for fast equilibration at low temperatures.

In comparison to liquid and supercooled liquid copper[20] which show only weak icosahedral order and very little temperature variation, Fe showed a monotonic increase in icosahedral order, which became very pronounced when supercooled. Analysis of quenched Fe revealed a natural way of introducing fivefold coordinated bonds plus a single −72° disclination line segment into an otherwise perfect bcc environment, without disturbing the surrounding structure. Addition of B to Fe decreased the icosahedral order, due to the positive disclinations centered on the smaller B atom which increased frustration. Further inclusion of larger Zr atoms to form FeZrB found an enhanced icosahedral order compared to FeB. This could possibly be explained by formation of negative disclination line defects[23] anchored on the larger Zr atoms, which eases the frustration of icosahedral order on the Fe atoms.

At high temperatures all of our measured structural properties of liquid Cu[20] and liquid Fe resembled each other, and also resembled a maximally random jammed[24] hard sphere configuration. This suggests that a nearly universal structure exists for systems whose energetics are dominated by repulsive central forces.

TABLE I. Details of tempering MD runs.

Chemical species	Temperatures (K)	Density ($Å^{-3}$)	Time (ps)
Fe_{100}	800–1900	0.0756	1.5
$Fe_{80}B_{20}$	700–1500	0.0814	1.8
$Fe_{70}Zr_{10}B_{20}$	700–1800	0.0787	1.8

Section II describes our combined method of Monte-Carlo and first principles MD, that we refer to as "tempering MD" and discusses other simulation details. Section III presents our results on pure Fe while (Sec. IV) compares this with FeB and FeZrB alloys.

II. TEMPERING MOLECULAR DYNAMICS (TMD) AND OTHER SIMULATION DETAILS

One reason alloys form glass more easily is that chemical identity introduces a new configurational degree of freedom that evolves slowly.[25,26] Unfortunately, this makes simulation more difficult. It is especially difficult to equilibrate the system at very low temperatures, because the probability to cross an energy barrier drops, trapping it in particular configurations. For this reason we use a Monte Carlo method, known as tempering or replica exchange[21,22] to augment our first-principles MD, allowing us to sample the configurational space more efficiently than conventional MD.

In the canonical ensemble, energy fluctuates at fixed temperature. A given configuration C with energy E can occur at any temperature T with probability proportional to $e^{-\beta E}$, ($\beta = 1/kT$). Now consider a pair of configurations, C_1 and C_2 of energy E_1 and E_2 occurring in simulations at temperatures T_1 and T_2. We can take C_1 as a member of the ensemble at T_2, and C_2 as a member of the ensemble at T_1, with a probability

$$P = e^{-(\beta_2-\beta_1)(E_1-E_2)} \tag{1}$$

without disturbing the temperature-dependent probability distributions of energy (or any other equilibrium property). Because each run remains in equilibrium at all times even though its temperature changes, we effectively simulate a vanishingly low quench rate.

In practice we perform several MD simulations at temperatures separated by 100 K. We use ultrasoft pseudopotentials,[27] using GGA exchange-correlation functionals, as provided with VASP[28] to perform the MD simulation. A "medium" precision setting as described in VASP has been used. This sets the plane-wave cutoff energy to 237.510 eV. All calculations are "Γ" point calculations (a single "k" point). All runs use an MD time step of 2 fs, and reach total simulated time of order 1.5–1.8 ps (see Table I) with a total of $N=100$ atoms. A larger time step of 2 fs does not affect the simulated liquid structure as is evident from our resulting liquid radial distribution function (Sec. III A). Every 10 MD steps we compare the energies of configurations at adjacent temperatures and swap them with the above probability. Eventually, configurations initially frozen at low temperature reach a higher temperature. The simulations then can carry the structure over energy barriers, after which the temperature can again drop. This comparison and swapping is done using a Perl script. The average swap rate is 0.43 for liquid Fe, 0.37 for FeB and 0.42 for FeZrB, indicating that parallel tempering is more efficient in sampling the phase space than simulated annealing. The convergence of the electronic steps is affected due to the frequent swapping. Every 10 MD steps when the *ab initio* simulation is restarted at all the temperatures, the convergence of the electronic degrees of freedom is longer for at least the first ionic step. This makes frequent swapping slightly inefficient in comparison to a single long first-principles MD. We suspect that this slow convergence may be due to the tightly bound d-shell electrons of Fe, since such slowing down of the electronic convergence was not observed in simulations of Cu or Al, but was observed in those of W.

In an effort to explore the structures of compounds with differing glass-forming ability we compare pure elemental Iron and two Iron-based glass-forming alloys. Tempering MD requires that we perform simulations at a constant density for all the temperatures, but we have no rigorous means of predicting the density at high temperature. For pure liquid Iron, the density is known experimentally,[29] and we use this value. For FeB and FeZrB, we took a high temperature liquid structure and quenched it, relaxing positions and cell lattice parameters, to predict a low temperature density. We then decreased the density of the relaxed structure by 6% to account for volume expansion, to arrive at the densities used in our liquid simulations.

The initial configurations at the twelve temperatures of FeZrB came from a previous tempering run at nine temperatures (700–1500 K) of 2 ps duration, which in turn came from a previous tempering run at six temperatures (1000–1500 K) of 2 ps duration. Short preliminary annealing was done at each newly introduced temperature before the beginning of a new tempering run. For FeB tempering, the starting configurations came from independent configurations of a long FeB MD run of about 3.3 ps at 1500 K with short preliminary annealing at the nine different temperatures.

Because of the efficient sampling of our tempering MD method, the structure of pure Fe partially crystallizes at low temperatures after about 1 ps. In the following discussion of our $T=800$ K sample we will refer to different structural features before and after crystallization. We also performed several long (2.0 ps) conventional first-principles MD at $T=800$ K yielding results similar to the results of tempering MD prior to crystallization.

For all runs we employed spin polarization, reasoning that local magnetic moments exist even above the Curie point. These local moments have a significant influence on the short-range order because ferromagnetic iron prefers a longer bond length than paramagnetic iron.[30] Of course, the ferromagnetic state of the liquid implies improper long-range correlations. Unfortunately, since our forces are calculated for electronic ground states, we cannot rigorously model the true paramagnetic state of liquid iron and iron-based alloys with these methods.

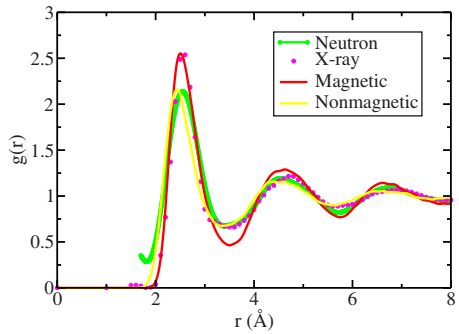

FIG. 1. (Color online) Radial distribution function of pure elemental liquid Fe. Simulations (magnetic and nonmagnetic) are run at $T=1800$ K, compared with x-ray experiments at $T=1833$ K (Ref. 29) and neutron scattering experiments at 1830 K (Ref. 31).

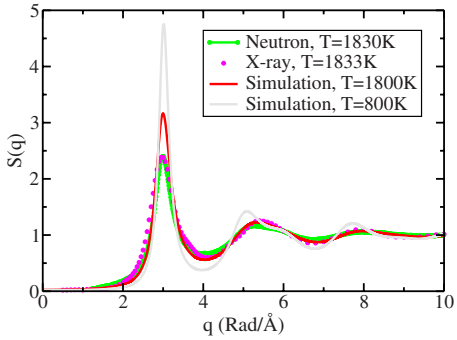

FIG. 2. (Color online) Comparison of simulated and experimental $S(q)$ near the melting temperature of Fe.

III. PURE FE

A. Radial distribution function $g(r)$

The radial distribution function, $g(r)$, is proportional to the density of atoms at a distance r from another atom and is calculated here by forming a histogram of bond lengths. We use the repeated image method to obtain the bond lengths greater than half the box size and anticipate $g(r)$ in this range may be influenced by finite size effects. Further, we smooth out the histogram with a gaussian of standard deviation 0.05 Å.

To evaluate the role of magnetism, Fig. 1 illustrates the radial distribution functions for liquid Fe simulated at $T=1800$ K, just below melting ($T_m=1833$ K). Evidently, the simulation with magnetism yields good agreement in the position and height of the first peak in $g(r)$ with experimental x-ray $g(r)$,[29] while neglect of magnetic moments results in near neighbor bonds that are too short and too weak. However, magnetism overestimates the strength of long-range correlations beyond the nearest-neighbor peak, while neglecting magnetism yields reasonably accurate long-range $g(r)$. Nevertheless, for the present study of local order, it is necessary to make spin polarized calculations to get the short range correlations and hence the local order correct. Strangely, a recent experimental neutron $g(r)$[31] has a shorter and broader first peak compared to both our magnetic $g(r)$ and to the $g(r)$ from the prior x-ray diffraction experiment.[29] The positions of the different maxima and minima in our simulated magnetic $g(r)$ compare well with both the experiments. The position of the first peak in our magnetic $g(r)$ is shifted by 0.05 Å to the left of the neutron first peak. The x-ray experiment doesn't have enough data points around the first maximum to determine the peak position accurately.

We calculate the coordination number by counting the number of atoms within a cutoff distance from a central atom. We choose the cutoff distance (R_{cut}) at the first minimum of $g(r)$. For pure Fe the minimum is at $R_{\text{cut}}=3.5$ Å. The precise location of the minimum is difficult to locate, and its variation with temperature is smaller than the error in locating its position, so that we do not change the value of R_{cut} with temperature. With this value of R_{cut} we find an average coordination number (N_c) of 13.2 which is nearly independent of temperature (N_c changes from 13.1 at high temperature to 13.3 with supercooling).

B. Liquid structure factor $S(q)$

The liquid structure factor $S(q)$ is related to the radial distribution function $g(r)$ of a liquid with density ρ by

$$S(q) = 1 + 4\pi\rho \int_0^\infty [g(r) - 1] \frac{\sin(qr)}{qr} r^2 dr. \tag{2}$$

One needs the radial distribution function up to large values of r to get a good $S(q)$. In our first principles simulation, we are restricted to small values of r, due to our small system sizes, so we need a method to get $S(q)$ from our limited $g(r)$ function. Baxter developed a method[32,33] to extend $g(r)$ beyond the size of the simulation cell. The method exploits the short range nature of the direct correlation function $c(r)$, which has a range similar to the interatomic interactions,[34] as opposed to $g(r)$ which is long ranged.

Assuming that $c(r)$ vanishes beyond a certain cutoff distance r_c, we solve the Baxter's equations iteratively to obtain the full direct correlation function for $0<r<r_c$. From $c(r)$ we calculate the structure factor $S(q)$ by a standard Fourier transform. The $S(q)$ showed good convergence with different choices of r_c. A choice of $r_c=5$ Å seemed appropriate because it was one half of our smallest simulation cell edge length. Even though in metals there are long range oscillatory Friedel oscillations, our ability to truncate $c(r)$ at $r_c=5$ Å shows that these are weak compared with short range interactions. An application of this method to obtain $S(q)$ of Cu[20] showed excellent agreement with the experimental $S(q)$.

The simulated $S(q)$ for pure Fe at $T=1800$ K (see Fig. 2) is compared to recent neutron scattering experiments at $T=1830$ K. Even though the positions of the different peaks compare very well, there is serious discrepancy in their heights. Especially, the height of the first peak of our simulated $S(q)$ is higher than that of the experiments. This discrepancy is expected because we include magnetism, which gives accurate short-range correlations while overestimating the long-range ones (see Fig. 1). But the cause of the dis-

TABLE II. $\hat{W}_6$ values for a few clusters. The Z8-Z16 series are Kasper polyhedra including the perfect icosahedron (Z12).

Cluster	No. of atoms	Voronoi type	$\hat{W}_6$
hcp	12	(0,12,0)	−0.012
fcc	12	(0,12,0)	−0.013
bcc	14	(0,6,0,8)	+0.013
Z8	8	(0,4,4)	+0.010
Z9	9	(0,3,6)	−0.038
Z10	10	(0,2,8)	−0.093
Z12	12	(0,0,12)	−0.169
Z14	14	(0,0,12,2)	−0.093
Z15	15	(0,0,12,3)	−0.037
Z16	16	(0,0,12,4)	+0.013

crepancy is not entirely clear since a comparison of the simulated structure factor of Ni[15] (done without including magnetism) with neutron scattering experiments[31] shows similar discrepancies between their $S(q)$'s.

A sum rule can be obtained for $S(q)$.[35,36] By inverting the Fourier transform of Eq. (2) and then taking the $r \to 0$ limit, one gets

$$I(Q) \equiv \int_0^Q q^2[S(q) - 1]dq \to -2\pi^2\rho \tag{3}$$

in the limit $Q \to \infty$. Further, the integral is supposed to oscillate with Q about the limiting value as $Q \to \infty$. Using our $S(q)$ we observed that the integral is consistent with the sum rule and oscillates nicely about the limiting value for $Q \geq 3$ Å^{-1}, while using the $S(q)$ from the neutron scattering experiments,[31] we observe a positive drift in the mean value about which the integral oscillates. Such a drift could indicate the presence of spurious background corrections. The $S(q)$ from the x-ray experiment[29] seems to be in good agreement with the ideal sum rule.

As we lower the temperature, the peak heights in $S(q)$ grow, indicating an increase in short range order with supercooling. We also observe a slight shoulder in the second peak of the $S(q)$ (Fig. 2), which grows with supercooling. The split second peak positions are in the ratios of 20:12 and 24:12 with respect to the first peak positions, just what one would ideally observe if there was icosahedral order.[23,37]

C. Bond orientation order parameter $\hat{W}_6$

Steinhardt *et al.*[6] introduced the $\hat{W}_l$ parameters as a measure of the local orientational order in liquids and undercooled liquids. To calculate $\hat{W}_l$, the orientations of bonds from an atom to its neighboring atoms are projected onto a basis of spherical harmonics. Rotationally invariant combinations of coefficients are then averaged over many atoms in an ensemble of configurations. The resulting measures of local orientational order can be used as order parameters to characterize the liquid structures. For an ideal icosahedral cluster, $l=6$ is the minimum value of l for which $\hat{W}_6 \neq 0$.

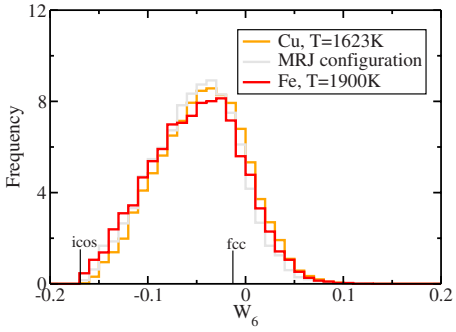

FIG. 3. (Color online) Distribution of $\hat{W}_6$ in liquid and supercooled liquid Fe and Cu. Fe shows more pronounced icosahedral order than Cu with supercooling.

Table II enumerates $\hat{W}_6$ values for different ideal clusters. The ideal icosahedral value of $\hat{W}_6$ is far from other clusters, making it a good icosahedral order indicator.

Kasper polyhedra[3,38,39] are polyhedra which minimize the number of disclinations for a particular coordination number. The series Z8-Z16 in Table II are such Kasper polyhedra but with the added constraint that the surface atoms be triangulated with equilateral triangles. The icosahedron with a coordination of 12 is one such Kasper polyhedron with no disclinations. Adding disclinations to the icosahedron, one finds that each disclination increases the $\hat{W}_6$ value by a similar amount irrespective of its sign.

As before, we choose the cutoff distance to specify near neighbors as $R_{cut}=3.5$ Å. For pure Fe at high temperatures, $\hat{W}_6$ resembles that of high temperature liquid Cu,[20] which in turn resembles the maximally random jammed configuration of hard spheres[24] (Fig. 3). On this basis we suggest that the MRJ configuration represents an idealized structure that is universal for strongly repulsive interactions. All pure metallic systems might approach this ideal structure at sufficiently high temperature.

However, as temperature drops the $\hat{W}_6$ distribution shifts strongly to the left, with a pronounced increase in $\hat{W}_6 \leq -0.1$ (Fig. 4). This indicates a rather high concentration of nearly icosahedral clusters in supercooled liquid Fe. Even at very low percentages of supercooling of Cu (~3%[20]) and Fe (~2%, not shown), Fe shows a clear enhancement in the negative $\hat{W}_6$ distribution as compared to Cu.

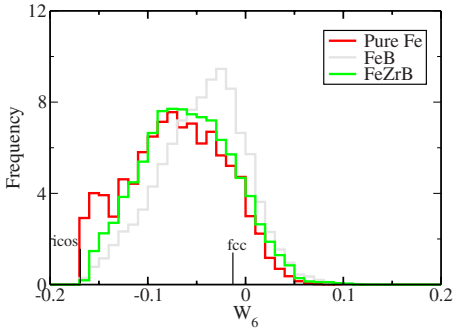

FIG. 4. (Color online) Distribution of $\hat{W}_6$ around Fe atoms, in supercooled Fe, FeB, and FeZrB at $T=800$ K.

TABLE III. Voronoi statistics (% of Fe atoms) for typical Fe-centered clusters in Fe, FeB, and FeZrB. Edges smaller than 0.33 Å and faces smaller than 0.3 Å^2 have been treated as a single vertex.

	Fe				FeB	FeZrB
	Supercooled liquid		Defective crystal		Supercooled liquid	Supercooled liquid
Voronoi type	800 K	Relaxed	800 K	Relaxed	800 K	800 K
(0,0,12)	8.3	11.0	5.0	0.0	0.6	1.4
(0,0,12,2)	2.1	3.6	2.0	2.0	0.5	0.3
(0,2,10,{0,1})	6.2	6.8	2.0	0.0	4.4	7.1
(0,1,10,2)	3.6	5.4	3.0	0.0	2.1	3.1
(0,4,8,{0,1,2,3})	7.9	4.8	10.0	6.0	8.6	9.4
(0,3,8,{0,1,2,3})	6.8	6.0	12.0	0.0	4.3	8.3
(0,2,8,{1,2,3,4})	3.0	3.0	3.0	0.0	0.0	0.0
(0,3,6,4)	2.1	2.2	2.0	6.0	0.0	0.0
(0,5,4,4)	1.5	1.2	3.0	18.0	0.0	0.0
(0,6,0,8)	0.0	0.4	0.0	56.0	0.0	0.0

We checked the $\hat{W}_6$ distribution of a nonmagnetic simulation to see if it is strongly influenced by magnetism, and found a nearly identical result. In particular, we still found a strong enhancement of the nearly icosahedral clusters relative to liquid Cu or pure Fe at high temperature.

D. Voronoi analysis

To explain the origin of this low $\hat{W}_6$ peak in pure Fe, we performed a Voronoi analysis[40] of the liquid before and during crystallization. A Voronoi polyhedron is described by indices $(F_3,F_4,F_5,\ldots)$ where F_i denotes the number of faces with i edges. For example $(0,0,12)$ denotes an icosahedron, while $(0,0,12,2)$ denotes a 14-coordinated (Z14) atom, with 12 fivefold bonds and 2 sixfold bonds. The $(0,0,12,2)$ is a characteristic tcp (tetragonal close-packed) structure of the Frank-Kasper type, with a $-72°$ disclination line running through an otherwise perfect icosahedron. In a body-centered cubic crystal all atoms are of Voronoi type $(0,6,0,8)$, which is an alternate 14-coordinated structure.

Supercooled liquid Fe at $T=800$ K (Table III) contains a high fraction of icosahedral atoms of type $(0,0,12)$ and $(0,0,12,2)$. Those with Voronoi type $(0,2,10,\{0,1\})$ and $(0,1,10,2)$ also have very negative $\hat{W}_6$, so that they can be thought of as related to the icosahedron. Together, they explain the enhanced negative $\hat{W}_6$ distribution. Supercooled Cu (which shows weak icosahedral order) and high temperature Fe ($T=1900$ K), in contrast contain about 1.2% of $(0,0,12)$ and no $(0,0,12,2)$. The MRJ configuration contains 1.2% $(0,0,12)$ but no $(0,0,12,2)$.

Strikingly, the icosahedral clusters tend to join in pairs and strings of three atoms in length. An instantaneous quench of a particular liquid structure at 800 K which had a high fraction of icosahedral units, using conjugate gradient relaxation of the atomic coordinates and lattice parameters, shows a clear enhancement of the icosahedral and other closely related units. The strings of icosahedral units found in the supercooled liquid connected to form networks. A quench starting from a different instantaneous supercooled liquid structure at 800 K containing fewer icosahedral structures resulted in rapid crystallization. This indicates that the presence of icosahedrons may inhibit crystallization. Similar quenches, starting from instantaneous liquid structures at higher temperatures, also resulted in relaxed structures with some of them showing a high negative $\hat{W}_6$ distribution comparable to the distribution at 800 K. The quenches that partially crystallized showed a high fraction of bcc $(0,6,0,8)$'s $(\sim 40\%)$ and were always accompanied by a high fraction of $(0,5,4,4)$'s $(\sim 25\%)$, which are otherwise absent or very low in the liquid.

Under TMD the supercooled liquid at $T=800$ K eventually crystallizes, with the $\hat{W}_6$ distribution peaked strongly around zero consistent with the value for ordinary crystalline clusters, but retaining a subset of atoms with nearly icosahedral $\hat{W}_6<-0.14$. Not surprisingly, these were precisely the atoms that had Voronoi type $(0,0,12)$ prior to crystallization. The Z14 $(0,0,12,2)$ atoms (with $\hat{W}_6\sim -0.093$) were mutual near neighbors, linked along their sixfold $(-72°)$ bonds, and also were neighbors of the nearly icosahedral atoms.

We quenched this sample by conjugate gradient relaxation of atomic coordinates and lattice parameters. After relaxation we found 56 atoms had bcc Voronoi type $(0,6,0,8)$. Six icosahedral atoms became 12-coordinated $(0,4,8)$ structures surrounding the bond connecting the two $(0,0,12,2)$ disclinated icosahedral atoms, which retained their type. The remaining atoms served to link the cluster of icosahedron-related atoms to the surrounding defect-free bcc crystal.

The icosahedron-related structure thus forms a point defect in an otherwise perfect bcc crystal. A simple way to create this defect is to take two consecutive triangles surrounding a near-neighbor bond along the bcc $[1,1,1]$ direction (see Fig. 5), displace them into the perpendicular bisecting plane and rotate by 30°. The atoms along the $[1,1,1]$ bond are now connected to each other by a sixfold bond

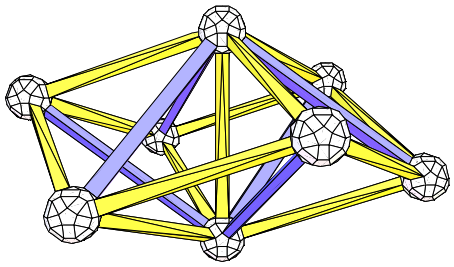

FIG. 5. (Color online) Fragment of BCC crystal illustrating a central bond in the [1,1,1] (vertical) direction, surrounded by two equilateral triangles rotated 60° from each other and displaced on either side of the midplane. Balls and sticks follow ZomeTool convention: Balls are icosahedral, yellow sticks are threefold, and blue sticks are twofold bonds.

(−72° disclination) and are connected to the six displaced atoms by fivefold bonds. This scheme to transform a bcc rhombic dodecahedron into a Frank-Kasper Z14 polyhedron was described in Refs. 41 and 42 in an attempt to explain certain diffraction anamolies in iron and vanadium-based alloys under ion irradiation.

Manually removing the defect, by reversing the above procedure then relaxing, yields a perfect bcc crystal with all atoms in a (0,6,0,8) Voronoi environment. We also embedded the point defect in an otherwise perfect bcc crystal with 128 atoms in a cubic box. Relaxation showed that the defect was stable. The energy of the defect was 6.18 eV and the fractional volume increase was 0.013.

Since tungsten, like iron, crystallizes in bcc, we performed a separate first-principles simulation of liquid tungsten. After supercooling by 13% to $T=3200$ K, we found the $\hat{W}_6$ histogram resembled that of Fe at 1600 K (which is 15% supercooled). A Voronoi analysis revealed a similar percentage of (0,0,12)'s and (0,0,12,2)'s in both these elemental bcc-forming metals. Hence we believe the relationship between bcc and icosahedral structures may be linked to our observed high fraction of icosahedra in liquid Fe as compared to Cu. This may also explain the reason why we are able to supercool bcc Fe more deeply than fcc Cu in our simulations.

We also included an icosahedron point defect inside an otherwise perfect fcc crystal of Cu, with 256 atoms in a cubic box. Relaxation showed that the defect was stable. The energy cost of the defect was 4.69 eV and the fractional volume increase was 0.012. Even though this fcc defect cost less energy than the point defect in bcc, and also needs little rearrangement of atoms as reflected by the slightly lower fractional density change, we do not see a significant icosahedral order in liquid Cu, when compared to liquid Fe. This could be because the number of icosahedrons that a single Z14 disclination can stabilize (up to six) is greater than one. So even an equal number of the two different defects in bcc and fcc would result in more icosahedral order in bcc than in fcc.

E. Honeycutt and Andersen analysis

Honeycutt and Andersen[5] introduced a useful assessment of local structure surrounding interatomic bonds. We employ a simplified form of their analysis, counting the number of common neighbors shared by a pair of near-neighbor atoms. This identifies the number of atoms surrounding the near-neighbor bond and usually equals the number of edge-sharing tetrahedra whose common edge is the near-neighbor bond. We assign a set of three indices to each bond. The first index is 1 if the root pair is bonded (separation less than or equal to R_{cut}). The second index is the number of near-neighbor atoms common to the root pair, and the third index gives the number of near-neighbor bonds between these common neighbors. We take the same value of $R_{cut}=3.5$ Å as mentioned before. Note that the Honeycutt and Andersen fractions depend sensitively on R_{cut}, making precise quantitative comparisons difficult.

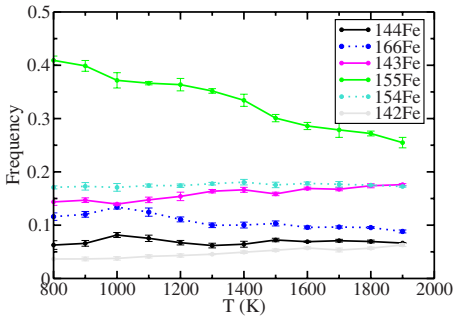

FIG. 6. (Color online) Honeycutt-Andersen analysis for pure Fe shows a clear increase in fivefold bonds with supercooling.

In general, 142's are characteristic of close packed structures (fcc and hcp) and 143's are characteristic of distorted icosahedra.[43] They can also be considered as +72° disclinations.[2–4] Likewise, 15's are characteristic of icosahedra, with 155's characterizing perfect icosahedra while 154's and 143's characterize distorted ones. 16's indicate −72° disclinations. 166's and 144's are also characteristic of bcc.

A Honeycutt and Andersen analysis for pure Fe, with an $R_{cut}=3.5$ Å (Fig. 6), showed that with supercooling the fraction of 15 bonds rises from 0.46 at $T=1900$ K to 0.59 at $T=800$ K in the liquid before crystallization. The fraction of 155's (characteristic of perfect icosahedra) was always larger than 154's (characteristic of distorted icosahedra), and seemed to be steeply increasing with supercooling as opposed to 154's, which were relatively flat. The fraction of 14 bonds drop from 0.32 to 0.30, with the icosahedral 143's being always higher than the cubic 142's. The 144's, which are characteristic of bcc remain nearly flat, even though the 166's show a slight increase. The ease of embedding a Z14 disclination in bcc Fe (see Sec. III D) might explain the slight increase in the 166's.

IV. Fe-B AND Fe-Zr-B

A. Radial distribution function $g(r)$

Figure 7 shows the pair correlation functions of supercooled FeZrB at $T=800$ K. From the heights of the first peaks, we see that the strongest bonds form between the metalloid (B) and the metal (Fe or Zr). The relative bond lengths reveal, as expected, that B behaves as a small atom,

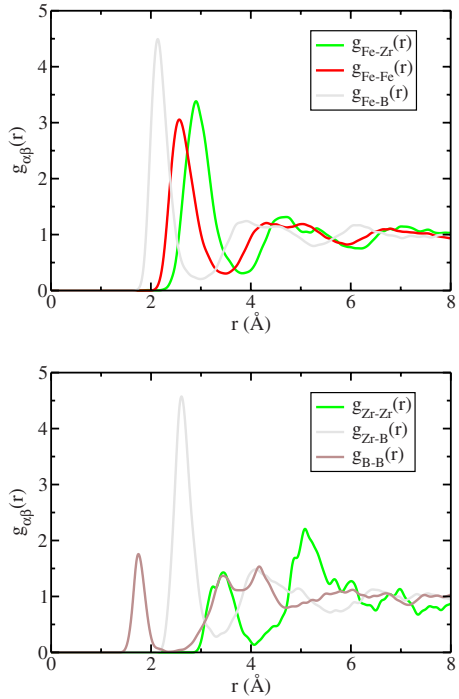

FIG. 7. (Color online) Partial radial distribution functions in FeZrB at $T=800$ K.

Fe is medium sized and Zr is large. Comparing simulations of FeZrB to pure Fe, we find that g_{FeFe} is reduced by alloying with B or ZrB, because Fe prefers to associate with B or Zr rather than with Fe.

To calculate the coordination number, define $N_{\alpha\beta}$ as the average number of atoms of type β around an atom of type α. We set R_{cut} at the first minima of the partial radial distribution functions (Fig. 7). We list the partial coordination numbers of FeB in Table. IV and FeZrB in Table V (averaged over all the temperatures since the temperature dependence is very weak and nonmonotonic). The average value of N_{FeFe} decreases with alloying, due to decrease in the concentration of Fe and the preference to bind with B and Zr. Zr, being a large atom, has a larger coordination number. Also note that B and Zr favor each other more than themselves. We do find some B-B pairs in the liquid state.

B. Liquid structure factor $S(q)$

Figure 8 shows the Faber-Ziman[44] partial structure factors of FeB at $T=800$ K, defined as

TABLE IV. Average coordination number in FeB. R_{cut} values are in angstrom units.

	FeFe	FeB	BFe	BB
R_{cut}	3.4	3.0	3.0	2.3
$N_{\alpha\beta}$	12.0	2.2	8.9	0.4

TABLE V. Average coordination number in FeZrB. R_{cut} values are in angstrom units.

	FeFe	FeZr	FeB	ZrFe	ZrZr	ZrB	BFe	BZr	BB
R_{cut}	3.4	3.8	3.0	3.8	4.0	3.3	3.0	3.3	2.4
$N_{\alpha\beta}$	9.5	2.0	2.0	14.0	0.9	2.8	6.8	1.4	0.4

$$S_{\alpha\beta}(q) = 1 + 4\pi\rho \int_0^\infty [g_{\alpha\beta}(r) - 1] \frac{\sin(qr)}{qr} dr. \qquad (4)$$

The positions of the first and second peaks in partial $S_{\mathrm{FeFe}}(q)$ is in very good agreement with the experimental results for amorphous FeB.[45] Also, at the position of the splitting of the second peak in $S_{\mathrm{FeFe}}(q)$, as observed in the experiments, we observe a slight shoulder. Similarly, the positions of the different peaks in $S_{\mathrm{FeB}}(q)$ and $S_{\mathrm{BB}}(q)$ are in agreement with the experiments.

For FeB, the $q \to 0$ limit of $S_{\mathrm{FeFe}}(q)$ is comparable to the experimental value. The $q \to 0$ limit in the other two partials differ from the experiment, $S_{\mathrm{BB}}(q)$ more seriously than $S_{\mathrm{FeB}}(q)$. We think that this discrepancy in the long wavelength regime is due to the very low density of B in our system which requires long times for equilibration of the alloys, and also leads to poor statistics. Nevertheless, the excellent agreement in the positions of the different peaks in the partial structure factors shows that we have reasonably good representative structures of FeB at $T=800$ K. Partial structure factors or partial pair distribution functions are not available experimentally to compare with FeZrB simulations.

C. Bond orientation order parameter $\hat{W}_6$

To define the $\hat{W}_6$ distribution in an alloy, we concentrate on central atoms of some particular species (e.g., Fe) but consider the neighboring atoms of all species. We chose the near-neighbor cutoff distances as before. Compare the Fe-based $\hat{W}_6$ distributions at their supercooled temperatures in Fig. 4. The origin of high negative $\hat{W}_6$ values for pure Fe was previously explained in Sec. III D. Replacing a few medium sized Fe atoms with smaller B atoms causes negative disclination lines to concentrate on Fe, leading to a drop in the

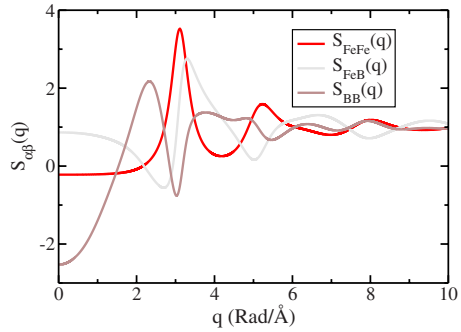

FIG. 8. (Color online) Simulated partial structure factors of FeB at $T=800$ K.

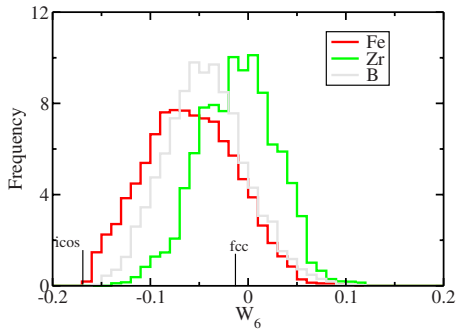

FIG. 9. (Color online) Distribution of $\hat{W}_6$ for different chemical species in supercooled FeZrB at $T=800$ K.

ideal icosahedral clustering on these Fe atoms and strongly reducing the extreme negative values of $\hat{W}_6$ in FeB. On the contrary, inclusion of Zr in FeZrB causes negative disclinations to attach to Zr, easing frustration, leading to more Fe centered clusters with icosahedral ordering and increasing the negative region of $\hat{W}_6$, as compared to FeB. Inclusion of the big Zr atom enhances icosahedral order on the Fe atoms.

Figure 9 shows the $\hat{W}_6$ distributions for FeZrB with centers at Fe, Zr, and B. The histogram with the center at Zr is almost symmetric about the value of zero. This suggests that the local environment about Zr atoms is nearly spherical, as is expected given its large size. The B centered $\hat{W}_6$ histogram is also asymmetric towards negative $\hat{W}_6$ values due to Kasper polyhedra and slightly distorted versions of them (see Table II and Sec. III C).

D. Voronoi analysis

A Voronoi analysis was performed for FeB in the supercooled liquid at $T=800$ K (Table III). The Fe environments were mostly $(0,4,8,x)$ or $(0,3,8,x)$ types, where $x=\{0,1,2,3,4\}$, with the higher coordination polyhedron being more favored. This was followed by the very negative $\hat{W}_6$ valued $(0,0,12)$, $(0,2,10,x)$'s and $(0,1,10,2)$'s Voronoi types occurring at lower frequency than in pure Fe. Boron mainly had environments of type $(0,3,6)$'s ($\sim$15% of B atoms) (Kasper polyhedron for $Z=9$ containing a +72° disclination) and $(0,5,4)$'s ($\sim$20%). These types are typical of the tricapped trigonal prism (TTP) and the monocapped square archimedean prism (a slightly distorted variant of TTP), respectively. The TTP is found in the crystal structures of Fe_3B with Pearson symbols oP16 and tI32. The distorted $(0,5,4)$ version is found in the structure $Fe_{23}B_6$ of Pearson type cF116. These structures have been identified as the leading competitors for B-Fe glass.[46] Boron also took environments of the Kasper polyhedron $(0,4,4)$ ($\sim$3%) corresponding to $Z=8$ and $(0,2,8)$ ($\sim$10%) corresponding to $Z=10$. The association of B with +72° disclinations explains how it increases the frustration of icosahedral order on the Fe atoms. Clearly the improved glass-formability of FeB compared with elemental Fe cannot be due to icosahedral order. Rather, it is presumed to be caused by the deep eutectic at $Fe_{83}B_{17}$.

TABLE VI. HA analysis for supercooled FeZrB at $T=800$ K.

	Root pair					
	Fe-Fe	Fe-Zr	Fe-B	Zr-Zr	Zr-B	B-B
14 pairs	**0.30**	**0.19**	**0.54**	**0.11**	**0.55**	**0.75**
142 pairs	0.08	0.06	0.03	0.06	0.03	0.02
143 pairs	0.17	0.11	0.35	0.04	0.33	0.33
144 pairs	0.05	0.02	0.17	0.01	0.19	0.41
15 pairs	**0.56**	**0.53**	**0.39**	**0.48**	**0.41**	**0.18**
154 pairs	0.22	0.27	0.03	0.36	0.04	0.0
155 pairs	0.33	0.22	0.37	0.08	0.36	0.17
16 pairs	**0.10**	**0.24**	**0.01**	**0.36**	**0.01**	**0.01**
166 pairs	0.09	0.20	0.0	0.26	0.00	0.00

A Voronoi analysis of supercooled FeZrB at $T=800$ K shows a clear increase in the very negative $\hat{W}_6$ polyhedra, and also a decrease in the number of Z14 $(0,0,12,2)$ types on Fe atoms indicating a decrease in frustration in the ternary as compared to the binary. Environments around B atoms were roughly similar in the binary and the ternary, with a slight increase in the lower coordinated ($Z=8$) Kasper polyhedra at the cost of higher coordinated ($Z=10$) ones. Zirconium took a variety of polyhedra, with an average coordination of 17.6 and a minimal coordination of 15, owing to its large size compared to the other constituents.

E. Honeycutt and Andersen analysis

We made a HA analysis of the ternary glassy alloy, by looking at root pairs of chemical species α and β, choosing R_{cut} in the manner of the $\hat{W}_6$ analysis. The frequency is normalized to sum to one for each species pair $\alpha\beta$. Table VI lists the fraction of different $1x$ pairs in supercooled FeZrB.

Among the $1x$ pairs with Fe as one of the root pairs, the 15's are most abundant at all temperatures. The 15's are mainly comprised of 155's and the 154's, with the 155's being always higher than the 154's. The percentage of 15's is similar for FeZrB, FeB as well as pure Fe. Note that the 15's are largest for the Fe-Fe pairs. They also show a steady enhancement with supercooling, unlike the 14's which decrease with supercooling. Among the 14's, the icosahedron-related 143's for all root pairs are always higher than the close-packed 142's, and remain fairly constant with supercooling. The 14's are maximal for FeB root pairs and minimal for FeZr.

Supercooled pure Fe has a high percentage of "16" 's (13%) compared to pure Cu (7%). The high number of "16" 's in Fe is related to the occurrence of Z14 $(0,0,12,2)$ environments in which the sixfold bond carries a −72° disclination, rather than the BCC 14 atom arrangement which would also show a high degree of fourfold and sixfold bonds (Sec. III D). Adding B to Fe, shows an increase of "16" 's for Fe-Fe pairs to 21% in FeB (not shown). Adding large Zr atoms to FeB decreases the occurrence of 16's on the Fe-Fe

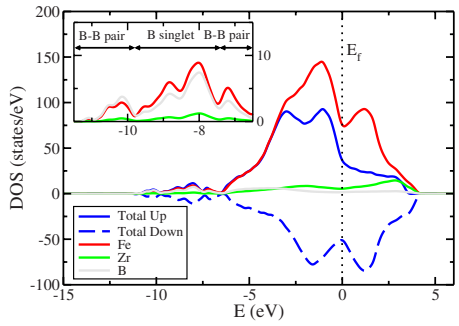

FIG. 10. (Color online) Average electronic density of states of quenched amorphous FeZrB at 0 K. Fe, Zr, and B partials include spin up and spin down states. The inset shows the low energy *s* states. The peaks below ~−10 eV and at ~−7 eV are due to B-B near-neighbor pairs.

pairs, putting them on Fe-Zr pairs and easing the frustration of Fe centers. This causes the geometry about Fe centers to be more icosahedral, and hence the shift of the $\hat{W}_6$ towards negative values.

Among the root pairs not containing Fe, note that the B-B pair has the maximum 14's (+72° disclinations), especially 144's, while the Zr-Zr pair has the maximum 16's (−72° disclinations), especially the 166's, emphasizing the role of size in controlling the frustration in alloys.

F. Electronic density of states of FeZrB

Since Fe and FeB density of states are available and their main features are also evident in FeZrB (Fig. 10), we focus our attention on the density of states (DOS) of the ternary, calculated using VASP. A $2\times2\times2$ *k*-point mesh was used to perform the calculations. A $3\times3\times3$ mesh preserves the low energy peaks in the DOS, indicating that they are not artifacts. The reported DOS is an average over the DOS of the final configurations of seven independent quenches.

The minority spin-down states are shifted from the majority spin-up states due to exchange splitting creating a pseudogap at the fermi level. Both the majority and the minority spin DOS show a further splitting reminiscent of the splitting between the T_{2g} and E_g-symmetry states in bcc iron,[47] but is also seen in other environments such as amorphous FeB.[48] The Fermi level falls in the T_{2g}/E_g-like pseudogap of the minority-spin density of states, a characteristic of strong magnetism.[49]

The Fe partial DOS (Fig. 10 shows combined spin up and down contributions) is similar to that of pure liquid Fe,[50] except that the features are broadened with alloying, since in the alloy there is also a compositional disorder in addition to structural disorder. The low energy Fe *d* states show some hybridization with the B *p* states. The Fe *s* states extend to very low energies and hybridize with the B *s* states. We observe this in FeB as well. The local DOS on neighboring B-B pairs shows a peak at ~−7 eV and at either of the two subpeaks just below ~−10 eV (see inset Fig. 10). The lower of these two subpeaks arise from B-B pairs of Honeycutt-Anderson type "15." Chains of B atoms, when present, occupy even lower levels around −11 eV. Other B atoms which do not have a B near neighbor are responsible for the remaining peaks between −8 eV and −10 eV. The Zr *s* states show weak correlation with the B *s* states. The Zr *d* states are largely unoccupied.

V. CONCLUSION

This study quantifies icosahedral and polytetrahedral order in supercooled liquid metals and alloys. This is the first such analysis of glass-forming Fe compounds using configurations from first-principles simulations. While the structural properties of Fe and Cu strongly resemble each other at high temperature, and indeed are close to a maximally random jammed structure,[20,24] their behavior evolves substantially, and in different manners, as the liquid is supercooled. Proper modeling of atomic interactions is essential to capture the differing behavior of each element, and use of a first-principles simulation is the most reliable means of achieving this.

For pure elements we find the degree of local icosahedral order in the supercooled liquid depends on the low temperature crystal structure, with bcc metals such as Fe and W accommodating icosahedra more readily than the fcc element Cu. Alloying with large or small atoms can further influence the degree of icosahedral order, with small atoms (e.g., B in Fe) aggravating the frustration by introducing positive disclination line defects, while large atoms (e.g., Zr in Fe) naturally stabilize negative disclination line defects, relieving frustration on the medium-sized Fe atoms. The enhanced glass-forming ability of FeB compared to Fe cannot be related to icosahedral order, even though, based on our findings, the possibility of relating it to other polytetrahedral order still remains open. But the enhanced glass formability of FeZrB compared to FeB can be explained by the formation of icosahedral order in addition to the expected slow dynamics of chemical ordering. Both of these factors possibly help in the destabilization of competing crystal phases in FeZrB.[46]

ACKNOWLEDGMENT

This work was supported in part by DARPA/ONR Grant No. N00014-01-1-0961.

[1] F. C. Frank, Proc. R. Soc. London, Ser. A **215**, 43 (1952).
[2] J. F. Sadoc and R. Mosseri, Philos. Mag. B **45**, 467 (1982).
[3] D. R. Nelson, Phys. Rev. Lett. **50**, 982 (1983).
[4] J. P. Sethna, Phys. Rev. Lett. **51**, 2198 (1983).
[5] J. D. Honeycutt and H. C. Andersen, J. Phys. Chem. **91**, 4950 (1987).
[6] P. J. Steinhardt, D. R. Nelson, and M. Ronchetti, Phys. Rev. B **28**, 784 (1983).
[7] T. Tomida and T. Egami, Phys. Rev. B **52**, 3290 (1995).
[8] C. Kuiying, L. Hongbo, L. Xiaoping, H. Quiyong, and H. Zhuangqi, J. Phys.: Condens. Matter **7**, 2379 (1995).
[9] B. Sadigh and G. Grimvall, Phys. Rev. B **54**, 15742 (1996).
[10] H. J. Lee, T. Cagin, W. L. Johnson, and W. A. Goddard, J. Chem. Phys. **119**, 9858 (2003).
[11] A. Pasquarello, K. Laasonen, R. Car, C. Lee, and D. Vanderbilt, Phys. Rev. Lett. **69**, 1982 (1992).
[12] G. Kresse and J. Hafner, Phys. Rev. B **48**, 13115 (1993).
[13] A. A. Valladares, J. Non-Cryst. Solids (to be published).
[14] D. Alfe, G. Kresse, and M. J. Gillan, Phys. Rev. B **61**, 132 (2000).
[15] N. Jakse and A. Pasturel, J. Chem. Phys. **120**, 6124 (2004).
[16] N. Jakse and A. Pasturel, Phys. Rev. Lett. **91**, 195501 (2003).
[17] N. Jakse, O. Lebacq, and A. Pasturel, Phys. Rev. Lett. **93**, 207801 (2004).
[18] N. Jakse, O. Le Bacq, and A. Pasturel, J. Chem. Phys. **123**, 104508 (2005).
[19] H. W. Sheng, W. K. Luo, F. M. Alamgir, J. M. Bai, and E. Ma, Nature (London) **439**, 419 (2006).
[20] P. Ganesh and M. Widom, Phys. Rev. B **74**, 134205 (2006).
[21] R. H. Swendsen and J. S. Wang, Phys. Rev. Lett. **57**, 2607 (1986).
[22] R. Yamamoto and W. Kob, Phys. Rev. E **61**, 5473 (2000).
[23] D. R. Nelson and M. Widom, Nucl. Phys. B **240**, 113 (1984).
[24] S. Torquato, T. M. Truskett, and P. G. Debenedetti, Phys. Rev. Lett. **84**, 2064 (2000).
[25] A. L. Greer, Nature (London) **366**, 303 (1993).
[26] P. J. Desre, Mater. Sci. Forum **179-181**, 713 (1995).
[27] D. Vanderbilt, Phys. Rev. B **41**, 7892 (1990).
[28] G. Kresse and J. Hafner, J. Phys.: Condens. Matter **6**, 8245 (1994).
[29] Y. Waseda, *The Structure of Non-Crystalline Materials* (McGraw-Hill, New York, 1980).
[30] E. G. Moroni, G. Kresse, J. Hafner, and J. Furthmuller, Phys. Rev. B **56**, 15629 (1997).
[31] T. Schenk, D. Holland-Moritz, V. Simonet, R. Bellissent, and D. M. Herlach, Phys. Rev. Lett. **89**, 075507 (2002).
[32] R. J. Baxter, J. Chem. Phys. **52**, 4559 (1970).
[33] D. J. Jolly, B. C. Freasier, and R. J. Bearman, Chem. Phys. **15**, 237 (1976).
[34] S. M. Foiles and N. W. Ashcroft, J. Chem. Phys. **81**, 6140 (1984).
[35] N. Norman, Acta Crystallogr. **10**, 370 (1957).
[36] J. Krogh-Moe, Acta Crystallogr. **9**, 951 (1956).
[37] S. Sachdev and D. R. Nelson, Phys. Rev. Lett. **53**, 1947 (1984).
[38] J. P. K. Doye and D. J. Wales, J. Phys. B **29**, 4859 (1996).
[39] F. C. Frank and J. S. Kasper, Acta Crystallogr. **11**, 184 (1958).
[40] J. L. Finney, Proc. R. Soc. London, Ser. A **319**, 479 (1970).
[41] V. S. Kraposhin, A. L. Talis, and J. M. Dubois, J. Phys.: Condens. Matter **14**, 8987 (2002).
[42] V. S. Khmelevskaya, V. S. Kraposhin, and V. G. Malynkin, Int. J. Non-Equilib. Process. **10**, 323 (1998).
[43] W. K. Luo, H. W. Sheng, F. M. Alamgir, J. M. Bai, J. H. He, and E. Ma, Phys. Rev. Lett. **92**, 145502 (2004).
[44] H. E. Fischer, A. C. Barnes, and P. S. Salmon, Rep. Prog. Phys. **69**, 233 (2006).
[45] E. Nold, P. Lamparter, H. Olbrich, G. Rainer-Harbach, and S. Steeb, Z. Naturforsch. A **36a**, 1032 (1981).
[46] M. Mihalkovic and M. Widom, Phys. Rev. B **70**, 144107 (2004).
[47] N. F. Mott, Adv. Phys. **13**, 325 (1964).
[48] J. Hafner, M. Tegze, and C. Becker, Phys. Rev. B **49**, 285 (1994).
[49] A. P. Malozemoff, A. R. Williams, and V. L. Moruzzi, Phys. Rev. B **29**, 1620 (1984).
[50] N. C. Bacalis, D. A. Papaconstantopoulos, M. J. Mehl, and M. Lach-hab, Physica B **296**, 125 (2001).